Electronic Supplementary Material (ESI) for Physical Chemistry Chemical Physics.
This journal is © the Owner Societies 2020

Supporting Information

Optimized Electronic structure and p-band centre control engineering to Enhance the Surface Absorption and Inherent Conductivity for Accelerated Hydrogen Evolution over Wide pH Range

Yuanzhe Wang, Dong Wang, Jiajia Gao, Xianfeng Hao, Zhiping Li, Junshuang Zhou, Faming Gao*

Key Laboratory of Applied Chemistry, College of Environmental and Chemical Engineering, Yanshan University, Qinhuangdao 066004, P. R. China.

*Corresponding author.E-mail: fmgao@ysu.edu.cn.

Experimental section

Materials Preparation

All chemicals were purchased from aladdin Co.,Ltd. and used as received.

As-MoS2 was fabricated via a facile one-pot hydrothermal method. Typically, 0.35 g of Na2MoO4, 2 g of thiourea, and 1 g of Arsenic sulfide (As2S2) were added to 43 mL of distilled water under vigorous stirring for 1 h to form a homogeneous solution. Then, the solution was transferred into a Teflon-lined stainless steel autoclave with a capacity of 75 mL for hydrothermal treatment at 350 ° C. After 6 h, the autoclave was naturally cooled down to room temperature ,and then the product was collected and washed with hydrochloric acid, distilled water and absolute ethanol several times to remove the impurities. Then, the product was dried in a vacuum oven at 70°C for several hours. Then, to determine the most suitable dosage of As2S2, 0.5 g and1.5 g of As2S2 were used. To explore the major impacts of nitrogen and phosphorus, N-MoS2, and P-MoS2 were also prepared by replacing As2S2 with C2H4N4 and NaH2PO2.

Materials Characterization

The microtopography and atomistic structural information of the samples were characterized by scanning electron microscopy (SEM, Carl Zeiss SUPRA 55 SAPPHIRE,15 kV), and transmission electron microscopy and (TEM, JEOL JEM-200EX 200 kV). Energy dispersive X-ray spectroscopy attached to the transmission electron microscope was used to obtain elemental contents. High-resolution transmission electron microscopy (HRTEM JEOL JEM-2010, 200kV)

and Raman spectroscopy (WITec, alpha300R, excited by a 512 nm laser) were also performed. X-ray diffraction (XRD) measurements were carried out using a Rigaku D/MAX-2500 powder diffractometer with Cu-K α radiation (λ = 0.154 nm) operated at 40 kV and 200 mA. X-ray photoelectron spectrum (XPS) was conducted using a Thermo Scientific ESCALAB 250Xi photoelectron spectrometer and Mg-Kα as the exciting source (1253.6 eV). Nitrogen adsorption-desorption isotherms were obtained on an ASAP 2020 HD88 (Micromeritics Instrument Corporation) instrument at 77K.

Electrochemical Measurements

All electrochemical measurements were performed in a standard three-electrode system using an electrochemical workstation (CHI760E). Typically, 5mg of the catalyst powders and 1 mg carbon black (Vulcan XC72) were dispersed in 1 mL of a water-ethanol mixed solvent (volume ratio of 3:1),along with 35 μL of Nafion solution, and the mixture was ultrasonicated for 1 h to form a homogeneous ink. Then, 20 μL of the prepared dispersion was drop onto the surface of a glassy carbon (GC) disk electrode (PINE AFE5T050GC) at a catalyst loading of 0.49 mg cm-2 . A graphite rod and SCE electrode were used as the reference and counter electrodes, respectively. Finally, the as-prepared catalyst was dried at room temperature. Linear sweep voltammetry and chronoamperometry with a scan rate of 5.0 mV s -1 were conducted in 0.5 M H2SO4 and 1.0 M KOH (purged with pure N2) using SCE as the reference electrode, respectively, graphite rod as the counter electrode. The electrochemical impedance spectroscopy (EIS) measurements were performed by applying an AC voltage with 5.0 mV amplitude in a frequency range from 106 to 0.1

Hz and recorded at -0.3 V (vs. SCE) in 0.5 M H2SO4. All the potentials were calibrated to a reversible hydrogen electrode (RHE) based on following equations:

E (vs. RHE) = E (vs. SCE) + 0.059×pH + 0.242 V.

MoS_2 edge oxidation

The preparation pristine MoS2 and As-MoS2 nanosheets is conducted by in situ negative linear sweeps from 0 to 0.9 V(vs. Hg/HgO) for five minutes at a scan rate of 5 mV s−1 in 1 M KOH solution before electrochemical measurements. Oxidation was confirmed by the observation of peaks at 232.4 and 235.5 eV from Mo6+ 3d5/2 and Mo6+ 3d3/2, respectively, using XPS.

Electrocatalytic HER mechanisms in acidic and alkaline solutions:
HER in acidic solution:

$H^+ + e^- + cat \rightarrow H^*\text{-}cat$	Volmer step
$2H^*\text{-}cat \rightarrow H_2\uparrow$	Tafel step
$H^*\text{-}cat + H^+ + e^- \rightarrow cat + H_2\uparrow$	Heyrovsky step

HER in alkaline solution

$H_2O + e^- + cat \rightarrow H^*\text{-}cat + OH^-$	Volmer step
$2H^*\text{-}cat \rightarrow H_2\uparrow$	Tafel step
$H^*\text{-}cat + H_2O + e^- \rightarrow cat + OH^- + H_2\uparrow$	Heyrovsky step

Theoretical Calculations

We performed first-principles calculations using the Vienna ab initio Simulation Package (VASP)[1,2] . All the results were obtained using the projector-augmented plane-wave (PAW) method within the Perdew, Burke, and Ernzerhof (PBE) parametrization scheme for the generalized gradient approximation (GGA) [3-5] . Monkhorst-Pack (MP) mesh of 3 × 3 × 3 is employed for geometry optimization. The pristine MoS2 monolayer is modeled by a 4×4 supercell with lateral size of

12.75×12.75 Å2, which contains 32 S and 16 Mo atoms. The distance between adjacent monolayers is 12.38 Å and hence the interaction between them can be eliminated. Full structural optimization was performed in which all lattice parameters and internal atomic positions were relaxed until the Hellmann-Feynman forces acting on each atom were less than 0.01 eV/Å and until the energy difference between two consecutive iterations was less than 0.0001 eV. Brillouin zone integrations were performed with a Gaussian broadening of 0.05 eV during all relaxations. For both structural and static electronic structure calculations, a plane-wave energy cut off of 400 eV was used for the GGA approach[6].

The free energy was calculated using the equation[7]:

$G = E + ZPE - TS$

where G, E, ZPE and TS are the free energy, total energy from DFT calculations, zero point energy and entropic contributions (T was set to be 300K), respectively.

The hydrogen adsorption energy in acidic solution is calculated as follows: $\Delta E_H = E(MoS_2+H) - E(MoS_2) - 1/2\ E(H_2)$, where $E(MoS_2+H)$ is the total energy of the non-metal atoms doped MoS2 with a hydrogen atom absorbed on the surface, $E(MoS_2)$ is the total energy for the non-metal atoms doped MoS_2 without an H atom absorbed and $E(H_2)$ is the energy for an H2 molecule in the gas phase. ΔG_H is calculated as ：

$\Delta G_H = \Delta E_H + 0.2eV$

The key reaction steps in alkaline HER:

The free energy for step ： $H_2O + e- + cat \rightarrow H^*\text{-}cat + OH^-$ and $H^*\text{-}cat + H_2O + e- \rightarrow cat + OH^- + H_2\uparrow$ should be the same at equilibrium potential of HER. Under

this assumption, one can avoid computation of the exact free energy of OH^- in solutions by using computational hydrogen electrode8. Herein, four main stage are considered: initial state, activated water adsorption, H* intermediates formation, H_2 formation[9]. The free energies in alkaline solution are calculated as:

$$G_0 = G_{\text{cat}} + G_{H_2O}$$

$$G_1 = G_{\text{cat-(H-OH)}^*}$$

$$G_2 = G_{\text{cat-H}^*} + G_{OH^-}$$

$$G_3 = G_{\text{cat}} + G_{OH^-} + \frac{1}{2} G_{H_2}$$

And $G_3 = G_0$.

Previous studies have proposed that there must be a balance between the transition state energies for water dissociation and the final state energies of adsorbed active species[10,11] . Herein, the ΔGH_2O (ΔGH_2O=G1-G0) value is applied as an activity descriptor for the Volmer step. And the species H-OH is a ground state of activated water adsorption. The ΔGH* (ΔG_{H*}= G2-G3) value is utilized as an activity descriptor for the Tafel step or Heyrovsky step[8,9].

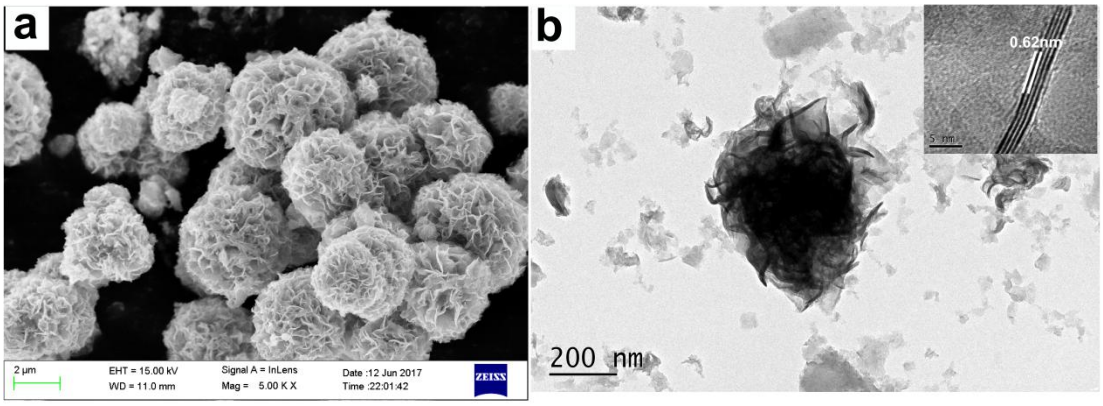

Fig. S1 Morphology characterization of the pristine MoS_2 catalysts.(a) SEM (b) TEM. The HRTEM is shown in the inset.

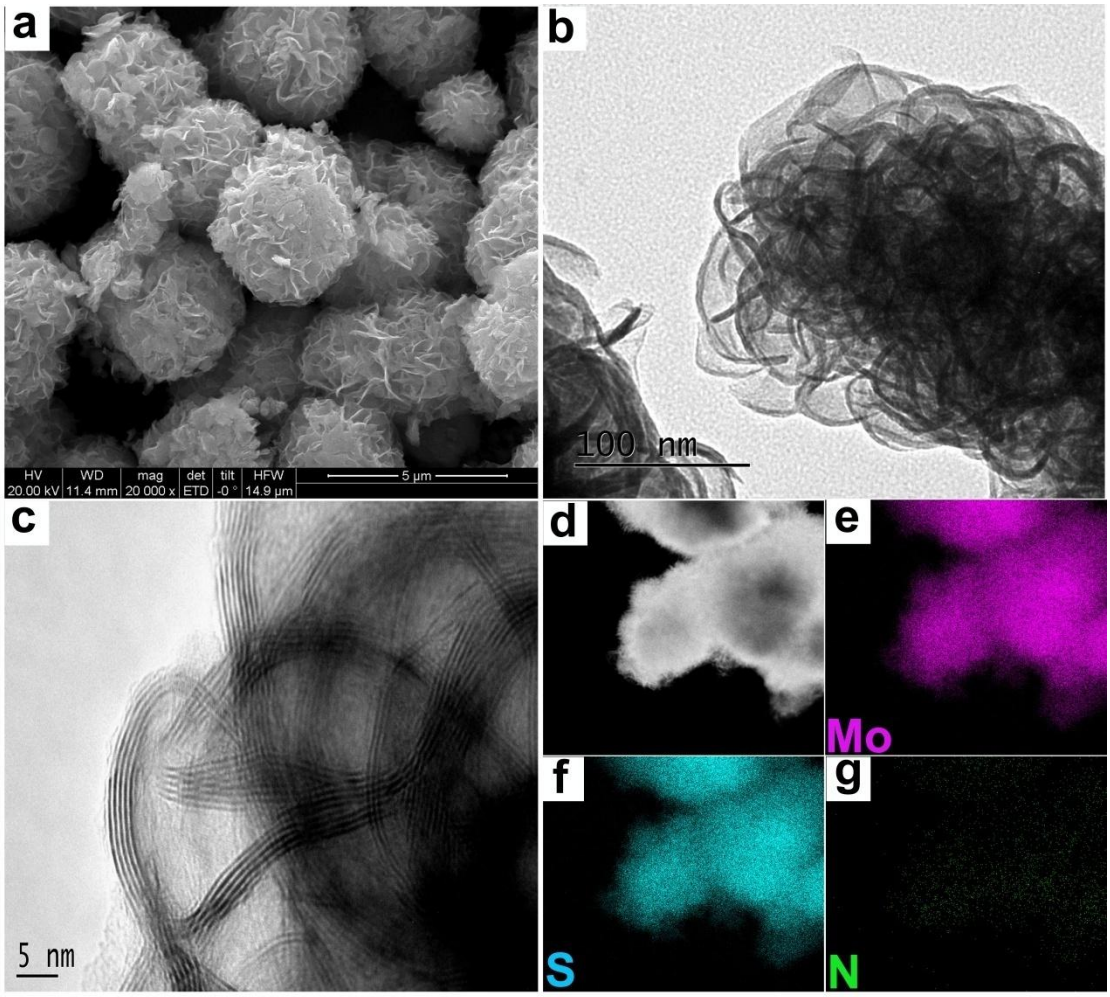

Fig. S2 Morphology characterization of the N-MoS_2 catalysts.(a) SEM (b) TEM and (c) HRTEM images of the N-MoS_2 nanosheets; (d-f) EDX elemental mapping of Mo, S, and N showing uniform distribution of the three elements

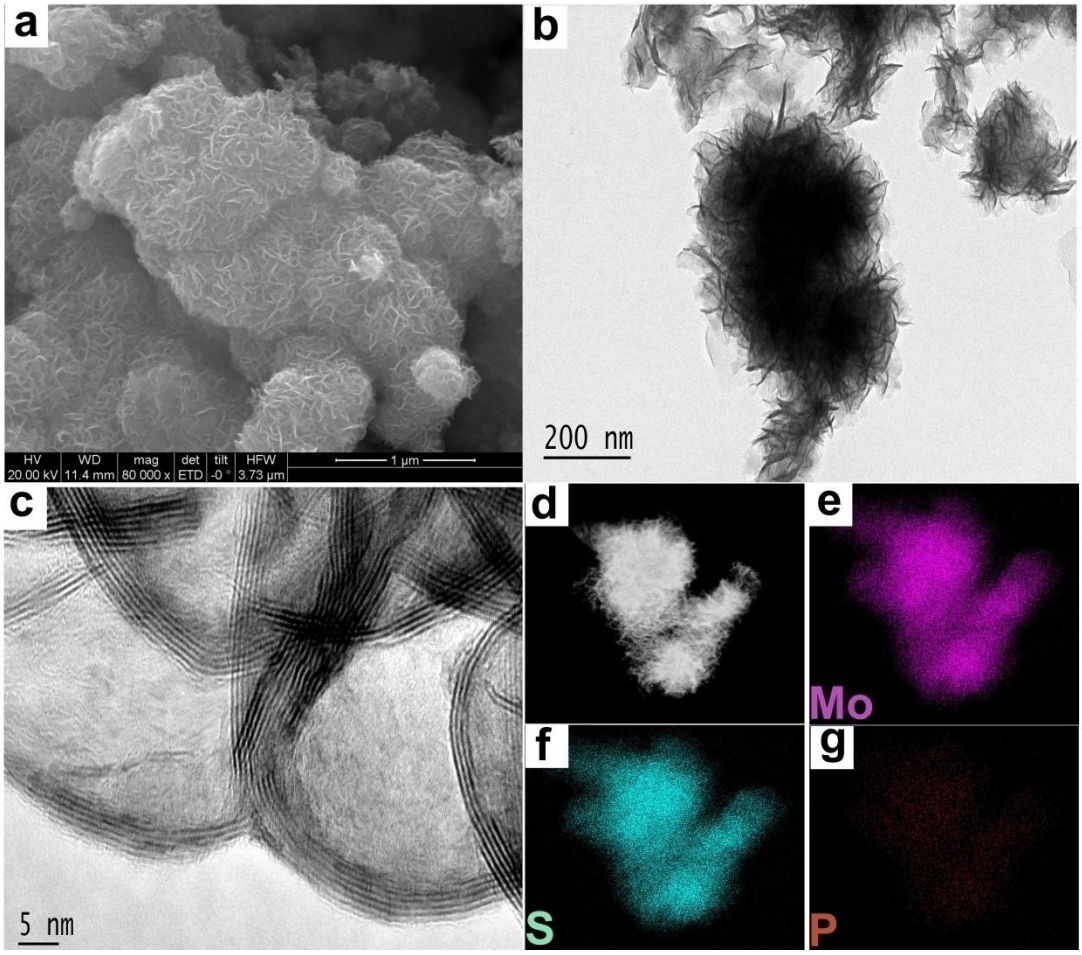

Fig. S3 Morphology characterization of the P-MoS_2 catalysts.(a) SEM (b) TEM and (c) HRTEM images of the P-MoS2 nanosheets; (d-f) EDX elemental mapping of Mo, S, and P showing uniform distribution of the three elements

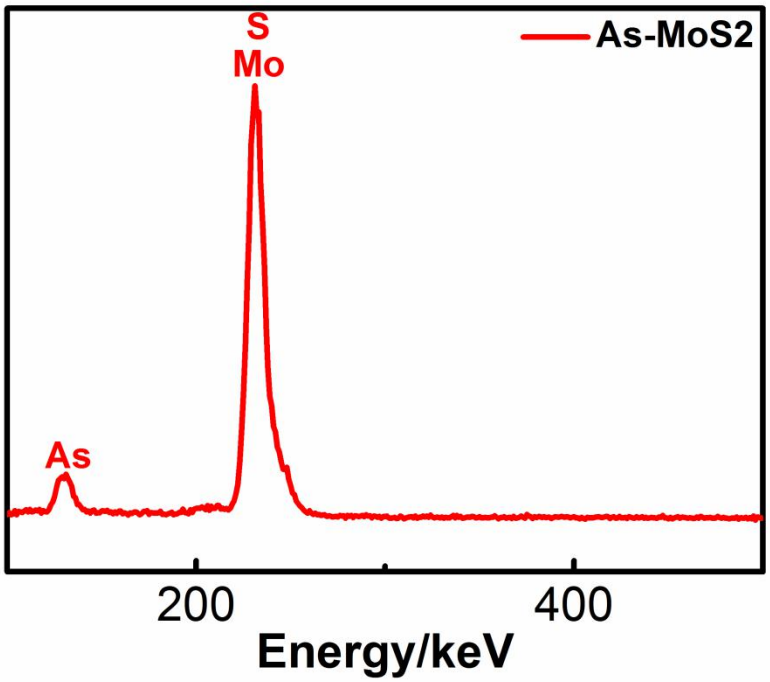

Fig. S4 EDX images of As-MoS_2

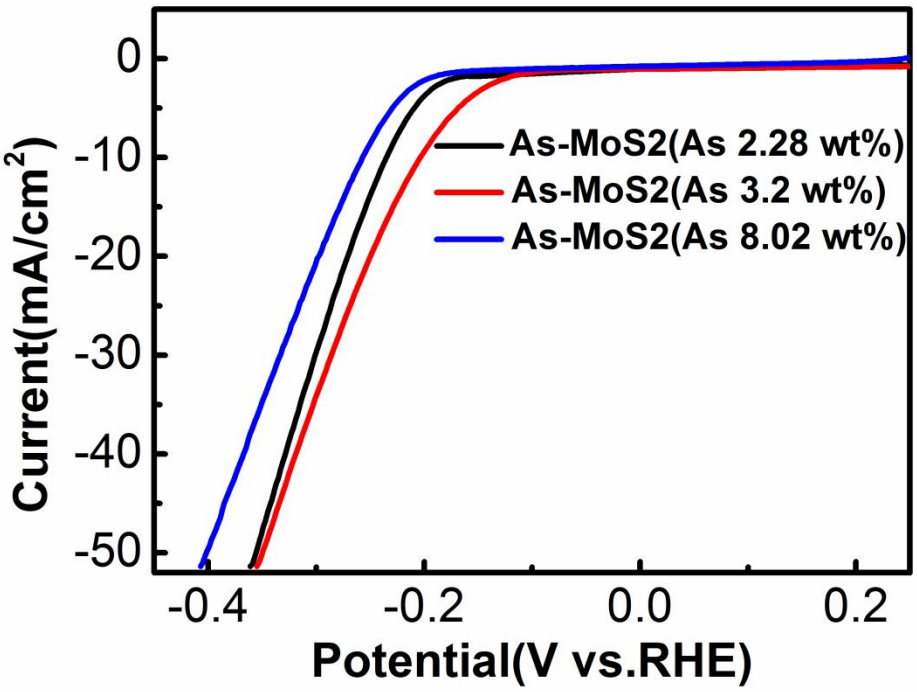

Fig. S5. Polarization curves of Electrochemical characterization of different dosage of As

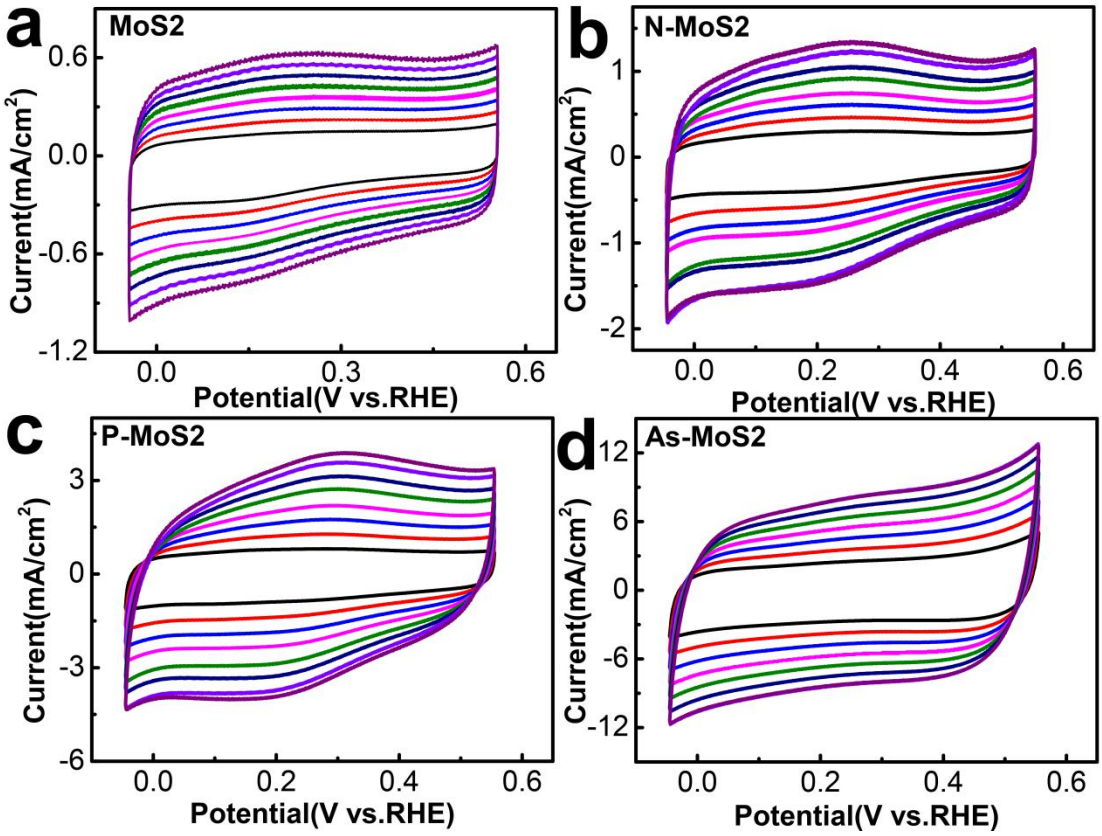

Fig. S6 (a-d)cyclic voltammograms with various scan rate from 40-160mVs $^{-1}$ at E =0.045−0.555V(vs RHE)

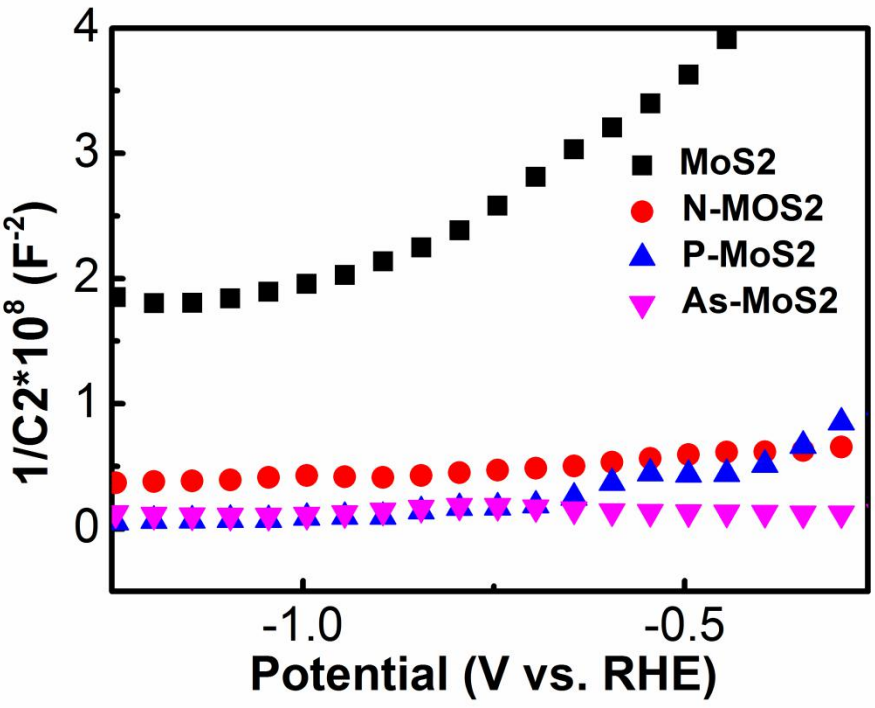

Fig. S7 Mott-Schottky plots for as-prepared MoS_2 nanosheets

Table. S1 The d-band-center of Mo atom for as-prepared samples

Samples	MoS2	B-MoS2	C-MoS2	N-MoS2	P-MoS2	As-MoS2
ε_d	-0.5159eV	-0.27eV	-0.42eV	-0.64eV	-0.49eV	-0.26eV

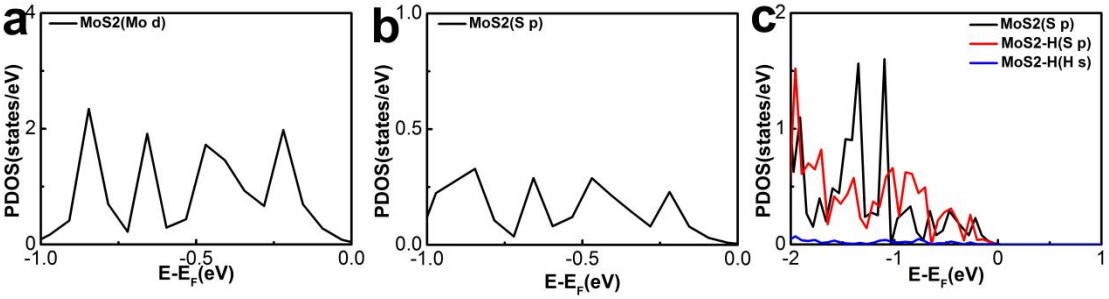

Fig. S8(a) Projected d-orbital density of states of Mo atoms for S connect sites. (b) Projected p-orbital density of states of S atoms for Mo connect sites. (c) Projected orbital density of states of S atoms prior to the H adsorption of pristine MoS_2 and subsequent to the H adsorption

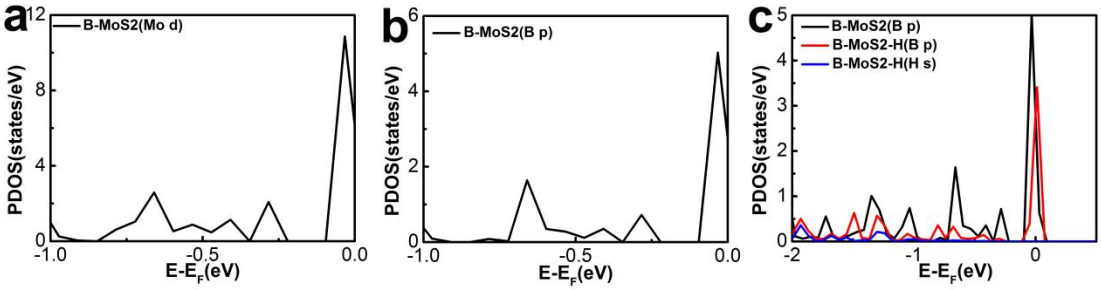

Fig. S9(a) Projected d-orbital density of states of Mo atoms for B connect sites. (b) Projected p-orbital density of states of B atoms for Mo connect sites. (c) Projected orbital density of states of B atoms prior to the H adsorption of B-MoS_2 and subsequent to the H adsorption.

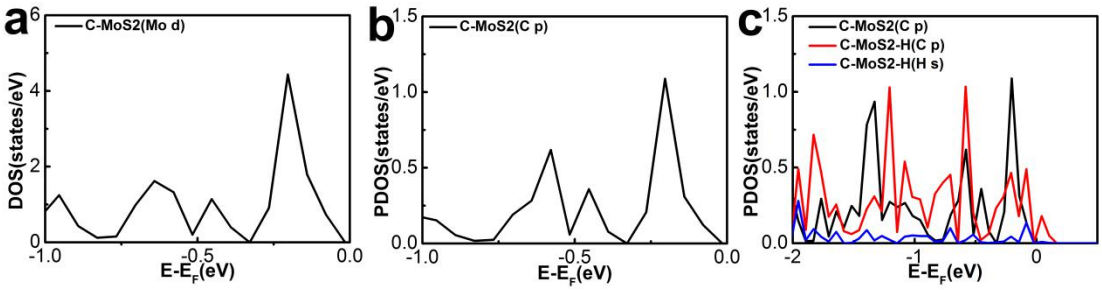

Fig. S10 (a) Projected d-orbital density of states of Mo atoms for C connect sites. (b) Projected p-orbital density of states of C atoms for Mo connect sites. (c) Projected orbital density of states of C atoms prior to the H adsorption of C-MoS_2 and subsequent to the H adsorption

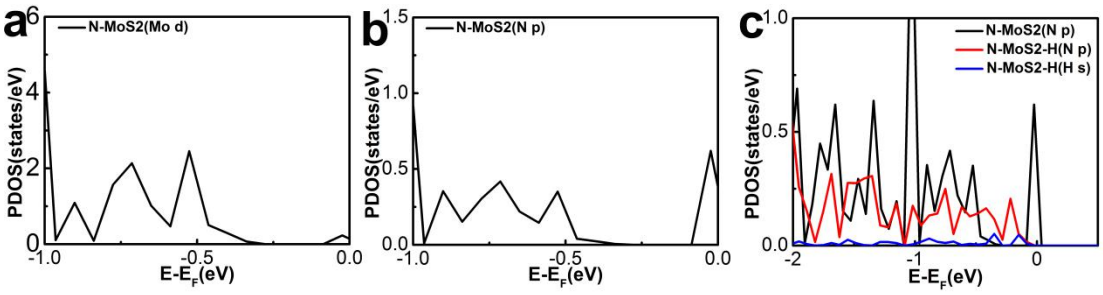

Fig. S11 (a) Projected d-orbital density of states of Mo atoms for N connect sites. (b) Projected p-orbital density of states of N atoms for Mo connect sites. (c) Projected orbital density of states of N atoms prior to the H adsorption of N-MoS_2 and subsequent to the H adsorption

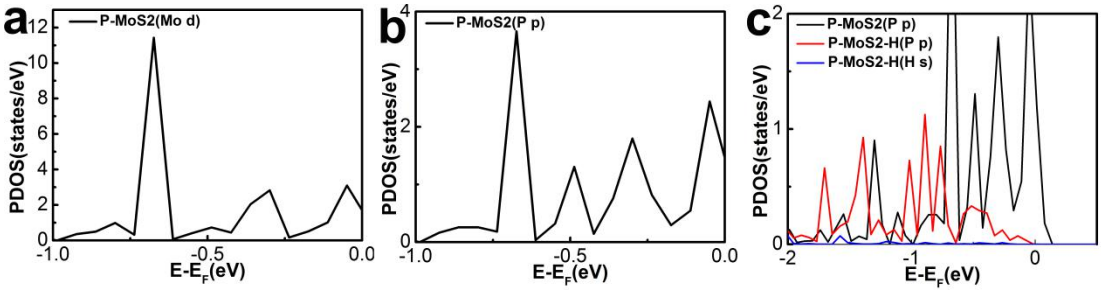

Fig. S12 (a) Projected d-orbital density of states of Mo atoms for P connect sites. (b) Projected p-orbital density of states of P atoms for Mo connect sites. (c) Projected orbital density of states of P atoms prior to the H adsorption of P-MoS_2 and subsequent to the H adsorption

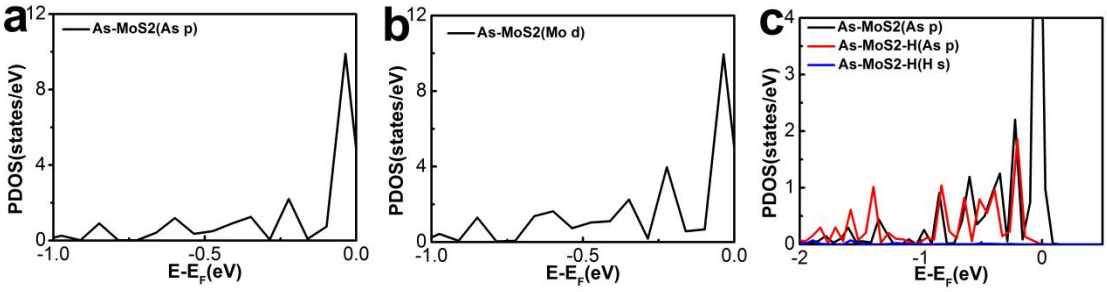

Fig. S13 (a) Projected d-orbital density of states of Mo atoms for As connect sites. (b) Projected p-orbital density of states of As atoms for Mo connect sites. (c) Projected orbital density of states of As atoms prior to the H adsorption of As-MoS_2 and subsequent to the H adsorption

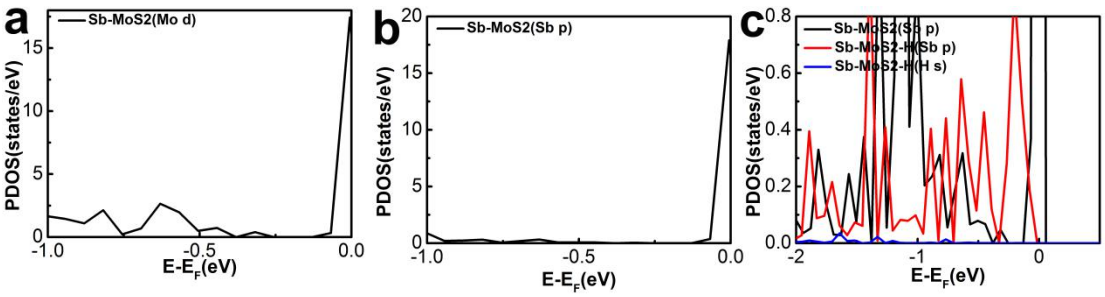

Fig. S14 (a) Projected d-orbital density of states of Mo atoms for Sb connect sites. (b) Projected p-orbital density of states of Sb atoms for Mo connect sites. (c) Projected orbital density of states of Sb atoms prior to the H adsorption of Sb-MoS_2 and subsequent to the H adsorption

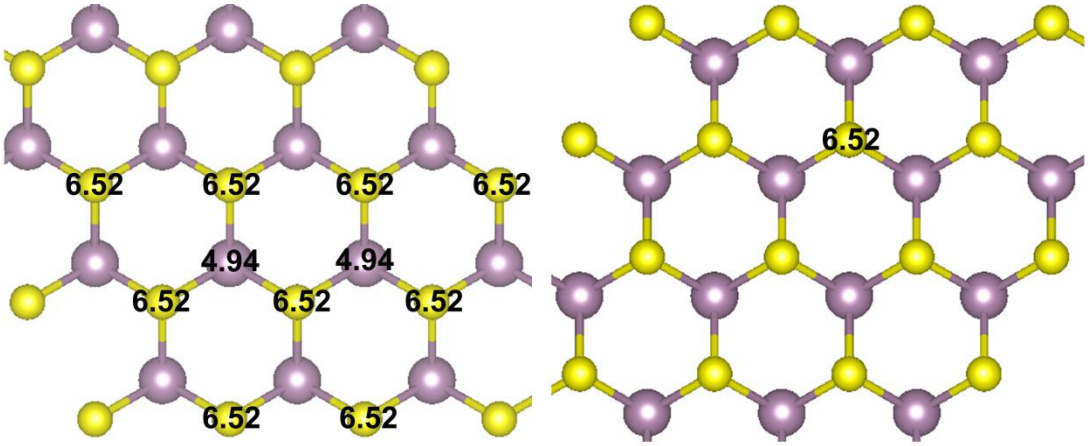

Fig. S15 Bader charge of different atoms for pristine MoS_2

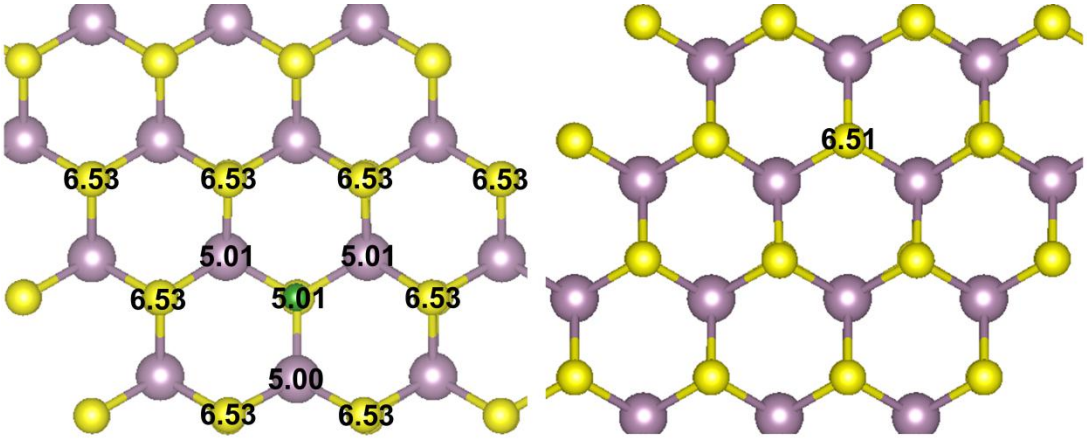

Fig. S16 Bader charge of different atoms for B-MoS_2

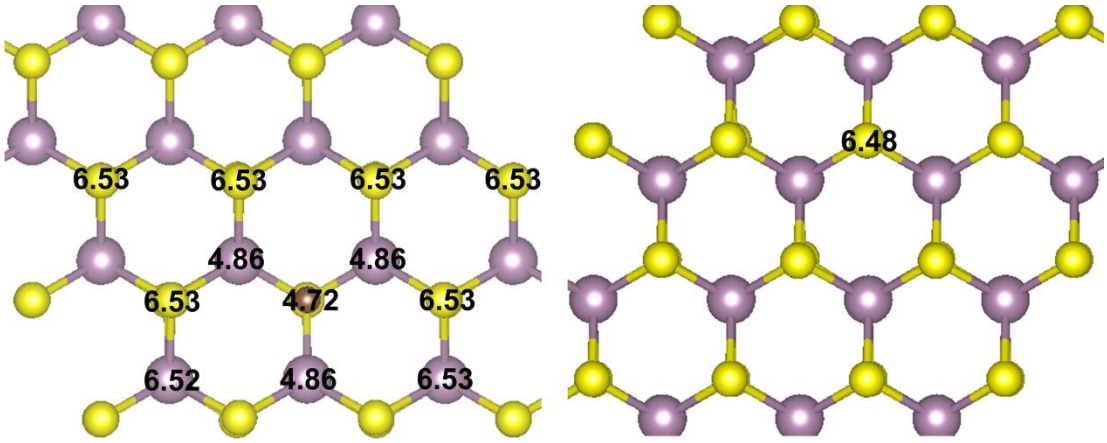

Fig. S17 Bader charge of different atoms for C-MoS_2

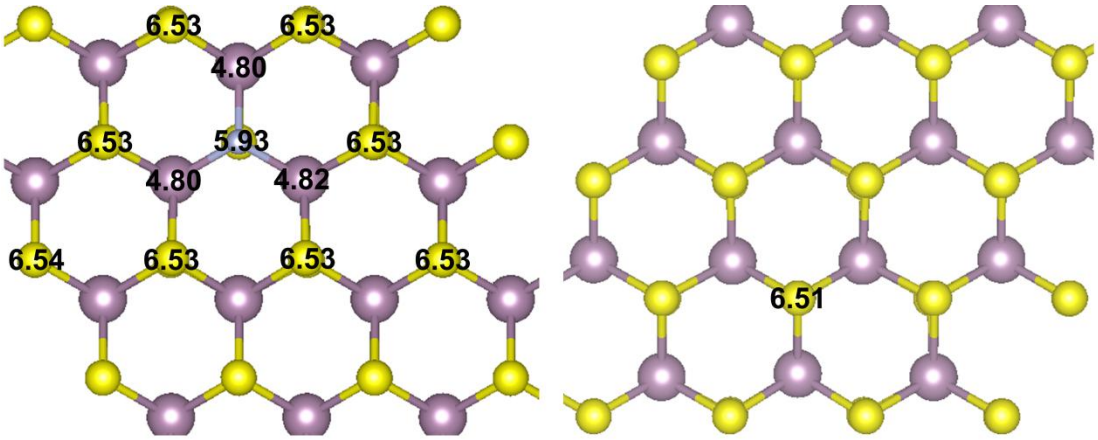

Fig. S18 Bader charge of different atoms for N-MoS_2

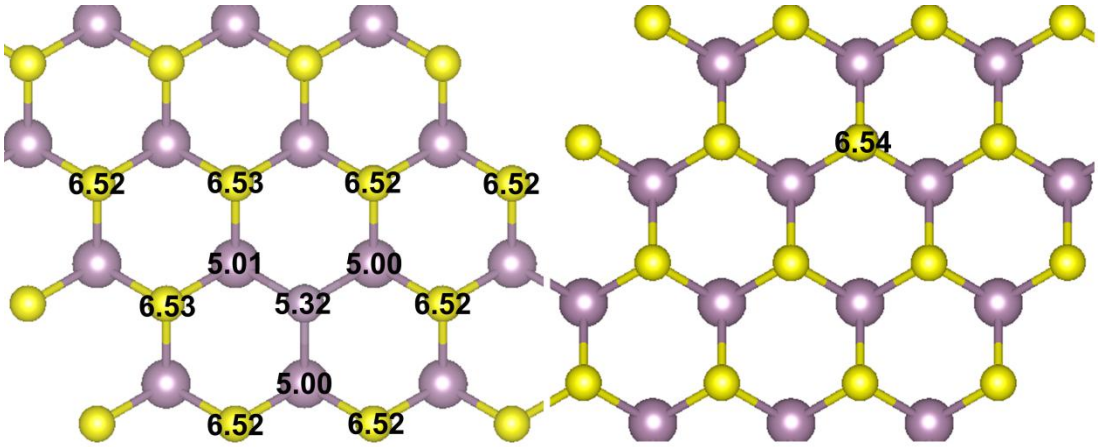

Fig. S19 Bader charge of different atoms for P-MoS_2

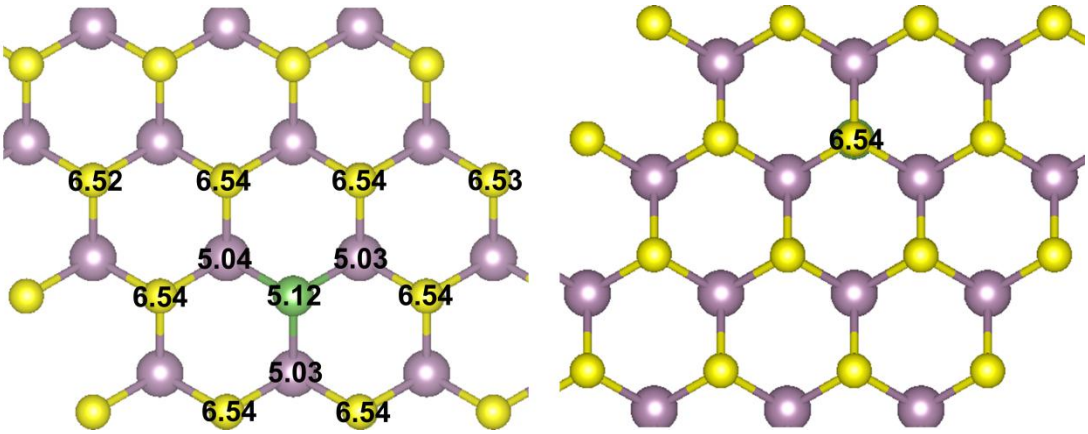

Fig. S20 Bader charge of different atoms for As-MoS_2

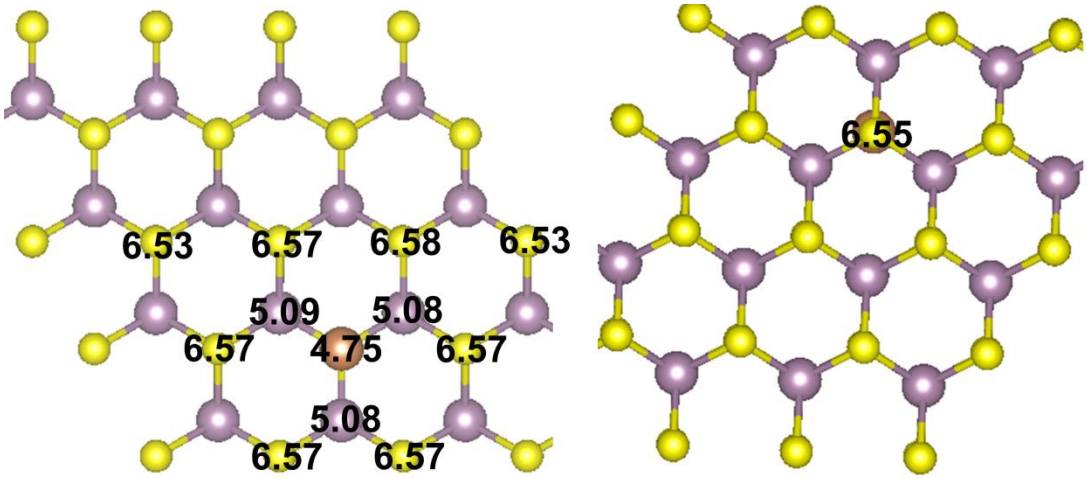

Fig. S21 Bader charge of different atoms for Sb-MoS_2

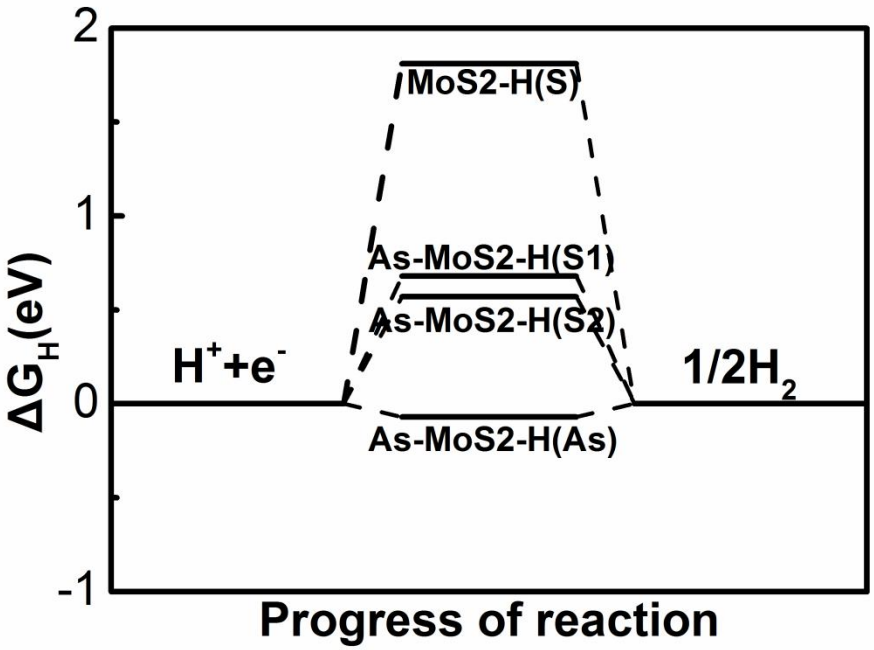

Fig .S22 HER free energy diagram for different S sites in the basal plane of As-MoS_2 nanosheets.

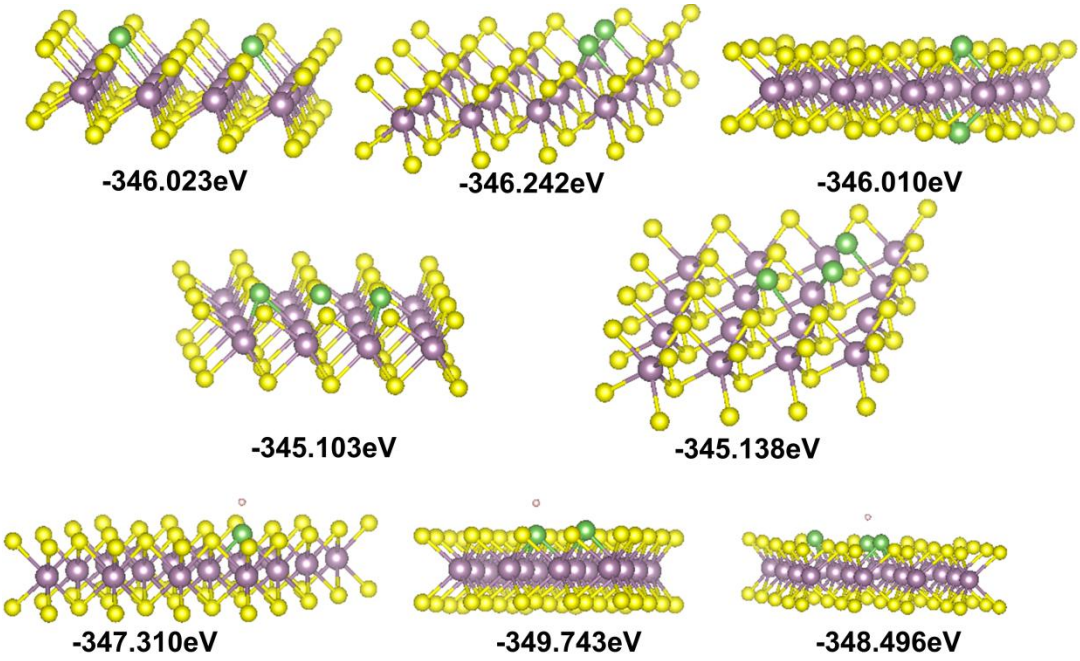

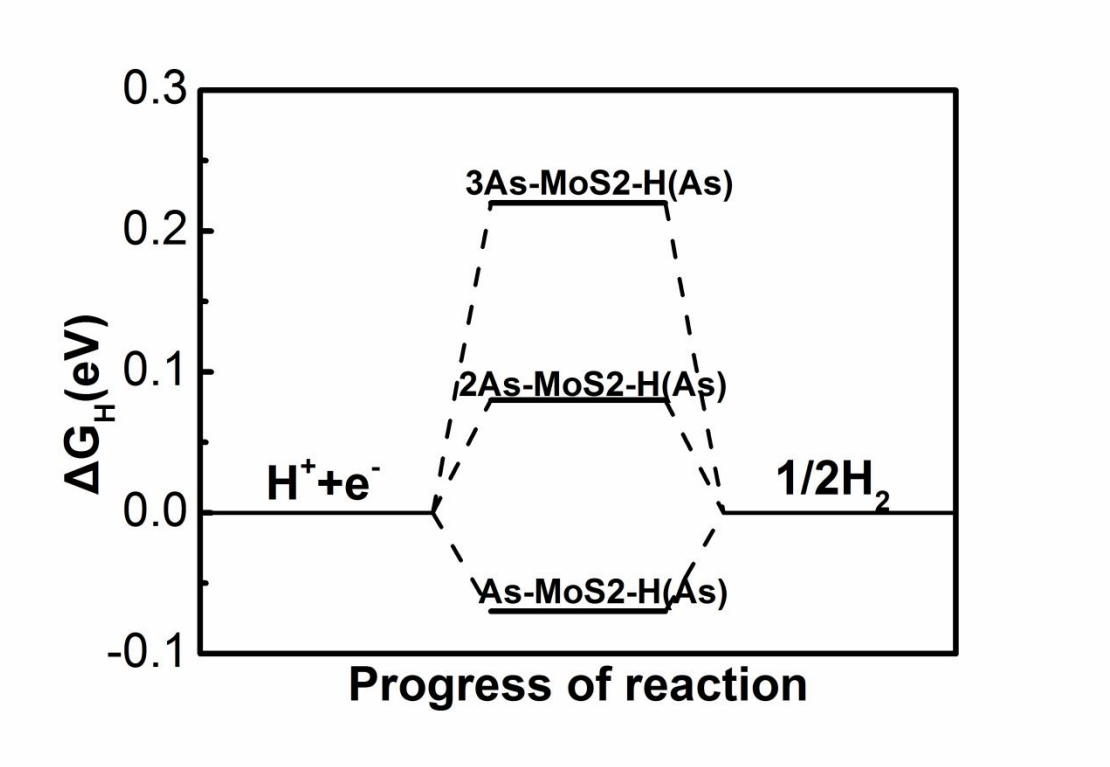

Fig. S23 HER free energy diagram for different dosage of As for As-MoS_2. The above are the corresponding atomic configurations.

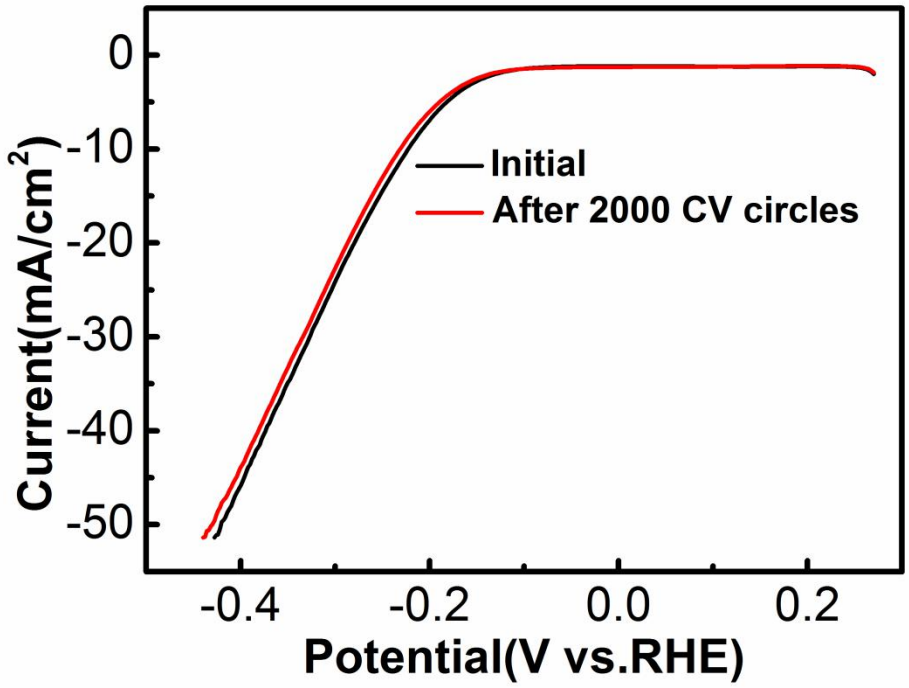

Fig. S24 LSV polarization curves for sample P-MoS_2 before (black line) and after (red line) 2000 CV cycles under alkaline solution

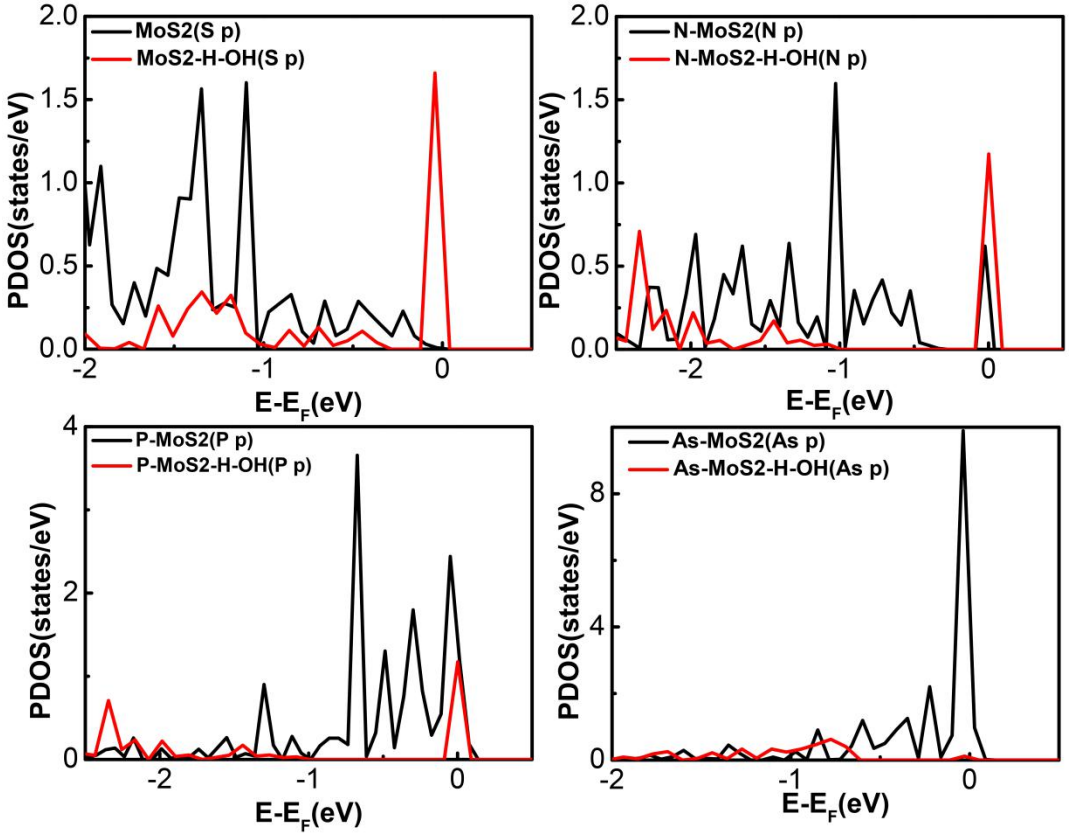

Fig. S25 Projected p-orbital density of states of atoms prior to the H2O dissociation adsorption and subsequent to the H2O dissociation adsorption. (a) pristine MoS_2. (b) N-MoS_2. (c) P-MoS_2. (d) As-MoS_2.

Table S2. Comparison of the HER performance of some Mo-based electrocatalysts in acdidic solution

Catalyst	**Catalyst amount** (mg/cm^2)	**Overpotential At 10mA cm^{-2}** (mV)	**Electrolyte**	**Reference**
mPF-MoS2	0.5	210	0.5M H_2SO_4	Nature Communications volume,8,
MoS2/CNT-graphene	0.65	255	0.5M H2SO4	Acs Nano,2014,8,5164
CoMoSx		≈210	H_2SO_4	Nat.Mater.2016,15,197
Defect-rich MoS2	0.285	195	0.5M H_2SO_4	Adv.Mater.,2013,2,5807
Exfoliated MoS2		195	0.5M H_2SO_4	J.Am.Chem.Soc.,2013,135,10274
Double-gyroid MoS2	0.06	≈260	0.5M H_2SO_4	Nat.Mater.2012,11,963
MoS_3/ CNTs		200	1 M H_2SO_4	Appl. Catal. B 135 (2013) 75e82
MoS_2/RGO		200	0.5 M H_2SO_4	Chem. Mater. 26 (2014) 2344e2353
fractal-shaped singlelayer MoS2		185	0.5 M H_2SO_4	10.1016/j.nanoen.2018.02.027
As-MOS2	0.49	200	0.5 M H_2SO_4	This work

Table S3 The concentration of elements in as-prepared samples

Catalyst	Mo（Atomic%）	S（Atomic%）	N（Atomic%）	P（Atomic%）	As (Atomic%)
MoS2	29.2	70.76	0.04	0	0
N-MoS2	27.63	69.55	2.82	0	0
P-MoS2	28.08	68.88	0.06	2.98	0
As-MoS2	28.05	68.67	0.08	0	3.20

Reference

[1] G. Kresse, J. Hafner, Phys. Rev. B47 (199) 5558-561.

[2] G. Kresse, J. Hafner, Phys. Rev. B49 (1994) 14251-14269.

[3] J. P. Perdew, K. Burke, M. Ernzerhof,Phys. Rev. Lett. 1996, 77, 3865.

[4] B. PE, Phys. Rev. B 50 (1994)17953-17979.

[5] G. Kresse, D. Joubert, Phys. Rev. B 59 (1999)1758-1775.

[6] Elsässer, C.; Fähnle, M.; Chan, C. T.; Ho, K. M. Phys. Rev. B. 1994, 49, 13975-13978

[7] J. K. Norskov, T. Bligaard, A. Logadottir, J. R. Kitchin, J. G. Chen, S. Pandelov and U. Stimming, PLoS One 5 (2005) e12154-e12154.

[8] Y. Zheng, Y. Jiao, Y. Zhu, L. H. Li, Y. Han, Y. Chen, M. Jaroniec and S. Z. Qiao, J. Am. Chem. Soc. 138 (2016) 16174-16181.

[9] J. Zhang, T. Wang, P. Liu, S. Liu, R. Dong, X. Zhuang, M. Chen and X. Feng, Energy Environ. Sci. 9 (2016) 2789-2793.

[10] D. Strmcnik, P. P. Lopes, B. Genorio, V. R. Stamenkovic and N. M. Markovic, Nano Energy 29 (2016) 29-36.

[11] R. Subbaraman, D. Tripkovic, K. C. Chang, D. Strmcnik, A. P. Paulikas, P. Hirunsit, M. Chan, J. Greeley, V. Stamenkovic and N. M. Markovic, Nat. Mater. 11 (2012) 550-557